

¹ High-Resolution NMR Spectroscopy in
² Microfluidic Droplets

³ William Hale, Gabriel Rossetto, Rachael Greenhalgh,
Graeme Finch, and Marcel Utz

⁴ January 16, 2019

Abstract

A generic approach is presented that allows high-resolution NMR spectroscopy of water/oil droplet emulsions in microfluidic devices. Microfluidic NMR spectroscopy has recently made significant advances due to the design of micro-detector systems and their successful integration with microfluidic devices. Obtaining NMR spectra of droplet suspensions, however, is complicated by the inevitable differences in magnetic susceptibility between the chip material, the continuous phase, and the droplet phases. This leads to broadening of the NMR resonance lines and results in loss of spectral resolution. We have mitigated the susceptibility difference between the continuous (oil) phase and the chip material by incorporating appropriately designed air-filled structures into the chip. The susceptibilities of the continuous and droplet (aqueous) phases have been matched by doping the droplet phase with a Eu³⁺ complex. Our results demonstrate that this leads to a proton line width in the droplet phase of about 3 Hz, enabling high-resolution NMR techniques.

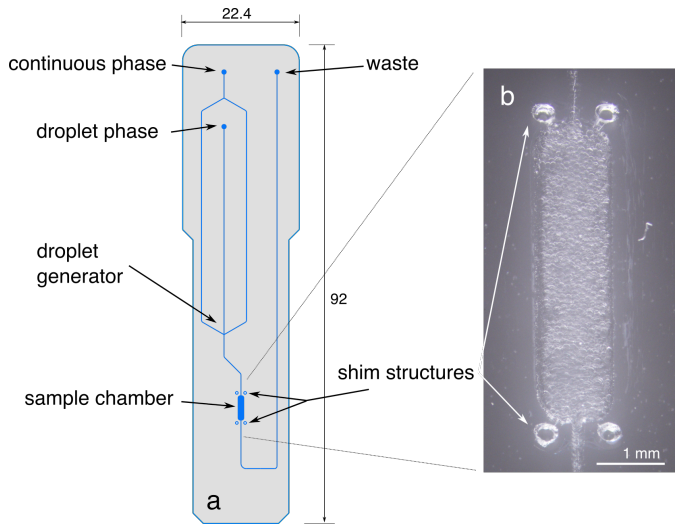


Figure 1: Droplet chip design (left) and detail micrograph of the sample chamber area filled with droplets (right). Some droplets are also visible in the entrance and exit channels.

21 Introduction

22 NMR spectroscopy is one of the most important analytical tools available to chemistry, biochemistry, and the life sciences. Due to its linearity and generality, it is particularly suited to quantify metabolic compounds in biological systems.^{1,2} At the same time, microfluidic technology is rapidly evolving, enabling numerous novel applications in chemistry and the life sciences. Droplet microfluidics is based on the separation of samples into small droplets suspended in an inert transport fluid (often a fluorinated oil).^{3–6} In this way, samples can be manipulated freely in the lab-on-a-chip (LoC) system, and problems due to viscous dispersion and cross-contamination are avoided. For example, several groups have reported encapsulation of cells into individual droplets.^{7,8} Droplets can efficiently be sorted according to numerous chemical and biochemical criteria by the help of suitable fluorescent markers. As a result, droplet microfluidic systems are increasingly finding applications in chemistry⁹ and the life sciences.^{8,10} In this paper, we explore the possibility to obtain high-resolution NMR spectra from small volumes of droplet emulsions.

sions on a chip. Integration of high-resolution NMR spectroscopy with microfluidic systems is challenging for a number of reasons. On the one hand, small sample volumes place stringent demands on detector sensitivity.^{11,12} This has recently been addressed with the design of highly efficient planar NMR microcoils¹³ and transmission line resonators.¹⁴

Another challenge is the preservation of high spectral resolution, which depends on a highly homogeneous magnetic field over the sample volume. Differences in magnetic susceptibility between the materials used for the microfluidic chip and the sample fluid, as well as the materials and geometry of the probe assembly, lead to a demagnetising field that varies continuously over the sample volume. Typical diamagnetic volume susceptibilities range from about -11 ppm to about -5 ppm (in SI units);^{15,16} differences of the order of several ppm are therefore commonplace. Unmanaged, they lead to broadening of NMR spectral lines over a ppm or more, which corresponds to a severe loss of resolution in ¹H liquid state NMR.

In emulsions, susceptibility differences between the oil and aqueous phases lead to similar line broadening.¹⁵ NMR spectroscopy is extensively used to characterise emulsion droplet size distributions using pulsed field gradient methods.¹⁷⁻²³ These methods do not require spectral resolution of individual compounds other than the two solvents, and are therefore unaffected by the susceptibility broadening. By contrast, high-resolution NMR spectroscopy, with sufficient resolution to distinguish multiple compounds present in either of the two phases, requires careful mitigation of the susceptibility differences.

We have recently shown that it is possible to compensate for susceptibility differences between microfluidic chips and the sample fluid by incorporating appropriately shaped shim structures into the chip design.²⁴ These structures are filled with air, and are shaped in such a way as to cause demagnetising fields that are equal and opposite to those caused

68 by the sample/chip interface. It has also been shown that susceptibility
69 differences can be compensated for in a liquid sample by doping of a
70 chelated lanthanide.²⁵ For example, Lennon *et al.* demonstrated that the
71 susceptibility mismatch between the inside and outside of deoxygenated
72 red blood cells could be compensated for by doping 3mM of dysprosium
73 tripolyphosphate (Dy(PPP)_2^{7-}) into the extracellular fluid.²⁶

74 Managing susceptibility differences for an emulsion of droplets on a
75 microfluidic chip adds additional complexity, since three different mate-
76 rials are now involved: the chip, the continuous phase, and the droplet
77 phase, all with different susceptibilities. In the following, we show that
78 this can be mitigated in a two-step approach, which is based on the obser-
79 vation that most organic solvents in use as continuous phases for droplet
80 microfluidics are less diamagnetic than water. First, the susceptibility
81 difference between the chip and the continuous phase are compensated
82 by shimming structures that are added to the chip design. Then, the
83 susceptibility of the aqueous droplet phase is matched to that of the
84 continuous phase by adding a paramagnetic solute.

85 It should be noted that in principle, the same effect could be achieved
86 if a diamagnetic dopant could be added to the continuous phase. How-
87 ever, while paramagnetic dopants are easily available in the form of tran-
88 sition metal ions, no effective diamagnetic dopants exist to our knowl-
89 edge.

90 Eu³⁺ complexes are paramagnetic, and are frequently used as shift
91 agents in NMR spectroscopy. Unlike other lanthanide ions such as Gd³⁺
92 or Ho³⁺, which are powerful nuclear relaxation agents, Eu³⁺ has only a
93 minimal effect on nuclear magnetic relaxation due to its extremely short
94 electron spin-lattice relaxation time.²⁷ Addition of millimolar quantities
95 of Eu³⁺ to aqueous solutions therefore does not cause significant relax-
96 ation line broadening, but changes the bulk magnetic susceptibility of
97 the solution proportionally to the Eu³⁺ concentration. It is therefore

Table 1: Bulk magnetic susceptibilities

<i>Compound</i>	$\chi_V/10^{-6}$ (SI)	Ref
water	-9.05	28
cyclohexane	-7.640	28
PMMA	-9.01	29
Air	+0.36	30

98 possible to adjust the susceptibility difference in a droplet emulsion by
 99 adding a Eu³⁺ complex that selectively dissolves in (or at least strongly
 100 partitions to) the aqueous phase.

101 In the present work, we use the diethyl-triamine pentaacetate (DTPA)
 102 complex of Eu³⁺, Eu[DTPA]²⁻. As an ion species, it is readily soluble
 103 in aqueous media, while exhibiting only negligible solubility in apolar
 104 organic solvents. Microfluidic chips are fabricated from poly methyl
 105 methacrylate (PMMA). By a fortunate coincidence, the susceptibilities
 106 of PMMA and water are very close to each other (Table 1). NMR lines
 107 in microfluidic devices made from PMMA are therefore narrow if aqueous
 108 samples are used, provided that the boundaries of the chip and the envi-
 109 ronment are either aligned with the external magnetic field, or are kept
 110 sufficiently remote from the detection area. By contrast, most organic
 111 solvents are considerably less diamagnetic than water, as exemplified by
 112 the case of cyclohexane, which has been used in the present study.

113 In the remainder of this paper, we first use finite element calcula-
 114 tions to estimate the NMR line widths expected in a droplet emulsion
 115 depending on the susceptibility mismatch. The results are then com-
 116 pared to experimental line widths obtained with varying concentrations
 117 of Eu[DTPA]²⁻ in the aqueous phase. Finally, we show that narrow
 118 NMR lines can be obtained by combining structural shimming²⁴ with
 119 susceptibility matching, and demonstrate that this approach can be used

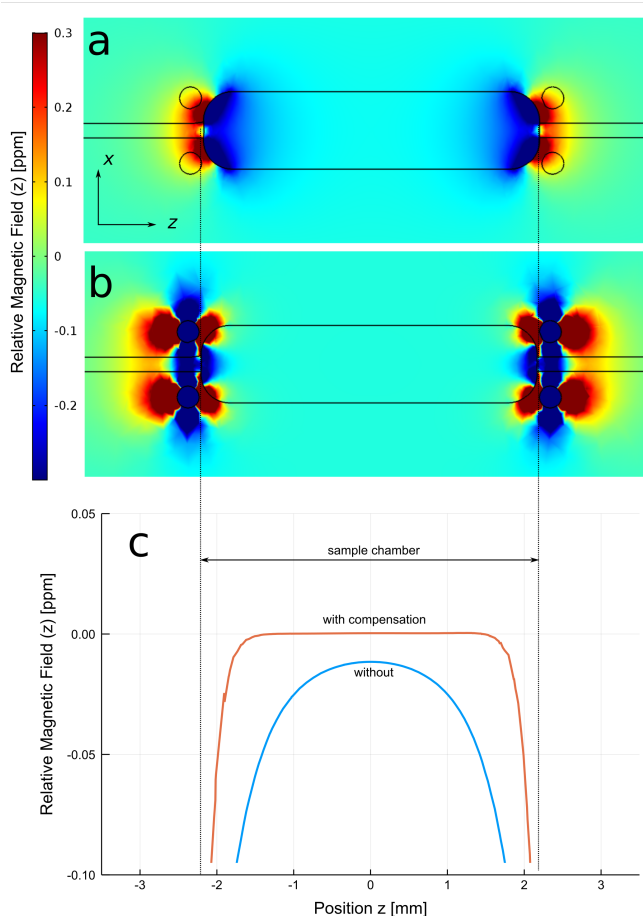


Figure 2: A: Finite element simulation of relative magnetic field distribution in an uncompensated chip (circular structures filled with PMMA) filled with cyclohexane and B: a compensated chip filled with cyclohexane; C: a linear plot of relative magnetic field along the z-axis through the middle of the sample chamber.

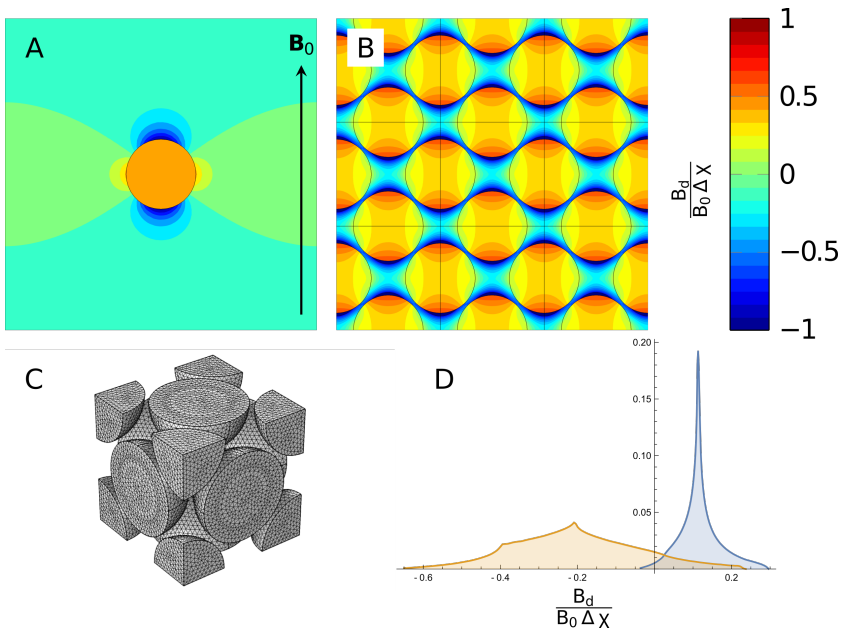


Figure 3: A: Finite element simulation of magnetic field distribution in droplets. z -component of the reduced magnetic field H_{red} in an isolated spherical droplet and B: in a face-centred cubic arrangement of droplets; C: FEM mesh used to calculate the result shown in B; D: histograms of the z -component of the reduced magnetic field in the continuous (orange) and in the droplet (blue) phase in the FCC arrangement.

120 to obtain a high resolution of glucose contained within the compensated
121 droplets. The chip used in this work is shown in Fig. 1. It consists of a
122 sample chamber in the centre of the chip, which is designed to line up
123 with the sensitive area of a transmission-line micro-NMR detector,¹⁴ and
124 a convergent flow droplet generator. The aqueous phase and the contin-
125 uous phase are fed into the two ports at the top. Droplets are formed
126 and transported downstream into the sample chamber. The chamber is
127 surrounded by four shim structures, which are circular shaped cutouts
128 filled with air. They have been designed to compensate for the difference
129 in susceptibility between the chip material (PMMA) and the oil phase
130 (cyclohexane) as shown in Fig. 2. The operation of the chip is shown on
131 the right side of Fig. 1; droplets of about 100 μm diameter are formed
132 and fill the sample chamber.

133 Materials and Methods

134 Microfluidic chips of the design shown in Fig. 1 were fabricated from
135 PMMA sheet material by laser cutting, and subsequent bonding of lay-
136 ers with a plasticiser under heat and pressure.³¹ The chips consist of a
137 top and bottom layer of 200 μm thickness each, and a middle layer of
138 500 μm . Fluid channels upstream from the flow-focussing droplet gen-
139 erator were scored into the middle layer at low laser power to a depth
140 of about 100 μm . Downstream from the droplet generator, the channels
141 and the sample chamber were cut through the 500 μm middle layer by
142 increased laser power, as were the shimming structures. The chips were
143 connected to a pair of Cole-Palmer 200-CE syringe pumps for droplet
144 generation. A flow rate of 20 $\mu\text{l}/\text{min}$ was typically used for the continu-
145 ous phase and 4 $\mu\text{l}/\text{min}$ for the aqueous droplet phase. The continuous
146 phase consisted of cyclohexane (Sigma-Aldrich) with 0.5% w/v of span-
147 65 (sorbitan tristearate, Sigma-Aldrich) as a surfactant to ensure droplet
148 stability. The cyclohexane/span solution was kept in a water bath at

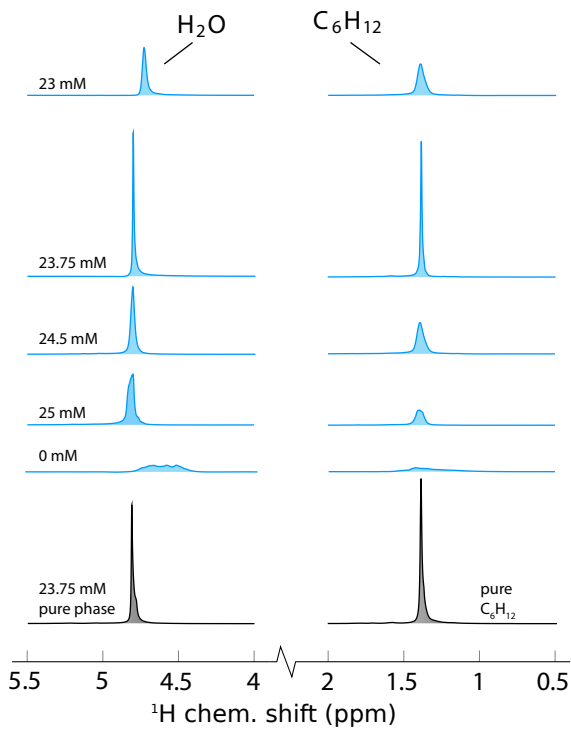


Figure 4: ^1H NMR line shapes of water (left) and cyclohexane (right) of a water in cyclohexane emulsion as a function of $\text{Eu}[\text{DTPA}]^{2-}$ concentration in the aqueous phase normalised to the sharpest peak. The spectra given in black are the pure phase spectra produced by the same chip.

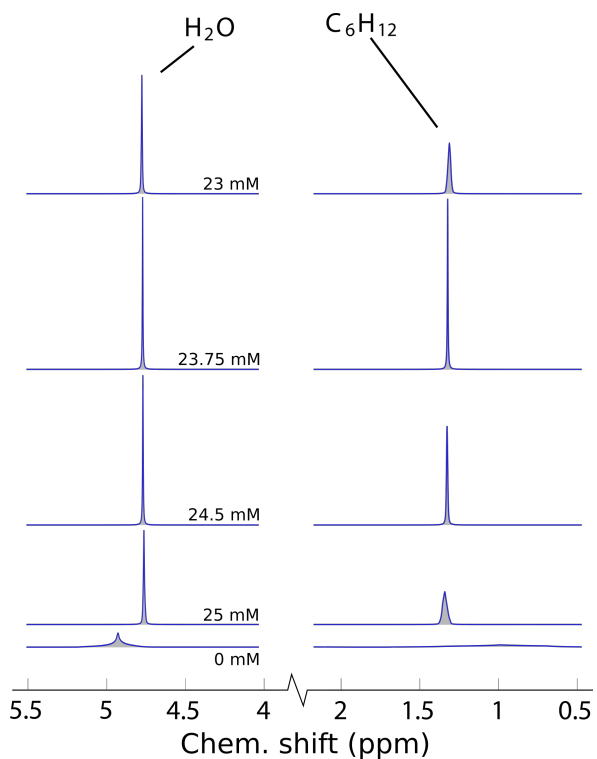


Figure 5: Predicted ¹H NMR line shapes of water (left) and cyclohexane (right) of a water in cyclohexane emulsion as a function of Eu[DTPA]²⁻ concentration in the aqueous phase.

149 30°C for at least 2h to ensure complete dissolution of the span. Prior to
150 use, all solutions were left to equilibrate at a controlled room temper-
151 ature of 25°C for at least 4h. Steady state conditions were ensured by
152 letting the droplet generation run until the volume inside the chip had
153 been exchanged at least five times. The chip was then disconnected from
154 the syringe pumps, and the connection points sealed prior to insertion
155 of the chip into the NMR probe.

156 NMR measurements were carried out on a Bruker AVANCE III spec-
157 trometer equipped with an Oxford wide bore magnet operating at 7.05
158 Tesla, corresponding to a ^1H Larmor frequency of 300 MHz. A home-
159 built NMR probe based on a transmission-line detector was used.¹⁴ It
160 accommodates microfluidic chips of the shape shown in Fig. 1. In the
161 present work, the probe was doubly tuned to allow irradiation both at
162 300 MHz for ^1H and at 75 MHz for ^{13}C . Details of the electronic and
163 mechanical design of the probe are given in Ref.³².

164 NMR spectra were obtained at an RF nutation frequency of 66 kHz
165 for ^1H , corresponding to 90 degree pulse length of 3.8 μs . Shimming
166 of the sample was first performed on a sample of pure cyclohexane in
167 an identical chip, these resulting values were used throughout all subse-
168 quent experiments with minor adjustments being made to linear shims
169 (X, Y, Z) before each experiment to minimise line width. NMR spec-
170 tra were acquired using Bruker spectrometer software (TopSpin 2.0),
171 and were processed using home-built scripts written in *Julia*.³³ 20 mM
172 of 4,4-Dimethyl-4-silapentane-1-sulfonic acid (DSS, Sigma Aldrich) was
173 added to the aqueous phase as a chemical shift standard.

174 MRI gradient echo images of the sample chamber were obtained using
175 ParaVision software and the fast low-angle shot (FLASH) pulse program.
176 Flip angles of 30° were employed as well as a repetition time of 600 ms;
177 8 scans were averaged for each image. Two images were acquired for
178 each field map at echo times of 6 and 10ms, respectively. The data was

¹⁷⁹ processed using home built software in *Mathematica*.

¹⁸⁰ Eu[DTPA]²⁻ solutions were prepared from a 82.2 ± 0.25 mM stock
¹⁸¹ solution, which was prepared by adding 1 g of EuCl₃ (Sigma Aldrich) to
¹⁸² a 50 mL volumetric flask. Separately, 3.93 g of diethylenetriaminepen-
¹⁸³ taacetic acid (DTPA, Sigma Aldrich) and 1.99 g of NaOH (Fischer) were
¹⁸⁴ dissolved in 100 mL deionised (DI) water (Sigma Aldrich) . An equimo-
¹⁸⁵ lar amount of the DTPA solution was added to the EuCl₃ solution. The
¹⁸⁶ pH of this solution was then adjusted by addition of 2M NaOH solution
¹⁸⁷ dropwise until a neutral pH was attained. This was then topped up to
¹⁸⁸ 50 mL using DI water.

¹⁸⁹ Finite element calculations of field distributions in emulsions were
¹⁹⁰ carried out using COMSOL Multiphysics with the "magnetic fields, no
¹⁹¹ currents" (mfnc) physics module. Optimisation of the shim structures
¹⁹² was done with COMSOL Multiphysics.³⁴ Starting from a SolidWorks
¹⁹³ model of the chip design, which was also used as a basis for production
¹⁹⁴ of the devices using a laser cutter, a finite element model was assem-
¹⁹⁵ bled and meshed. The shim structures consist of four symmetrically
¹⁹⁶ arranged circular holes through the middle layer of the three-layered de-
¹⁹⁷ vices. The positions and the diameters of these holes were optimised
¹⁹⁸ using a Nelder-Mead simplex algorithm. At each iteration, the magnetic
¹⁹⁹ field distribution inside the sample chamber was calculated using the
²⁰⁰ mfnc physics module. The square norm of the second derivative of the
²⁰¹ z-component of the magnetic field was integrated over the volume of the
²⁰² sample chamber, and was used as optimisation target.

²⁰³ Results and Discussion

²⁰⁴ While it is possible to predict the magnetic field distribution in a sys-
²⁰⁵ tem of multiple phases with differing susceptibilities by solving the mag-
²⁰⁶ netostatic equation, this requires precise geometric information on the
²⁰⁷ arrangement of the two phases. In the case of an emulsion, the arrange-

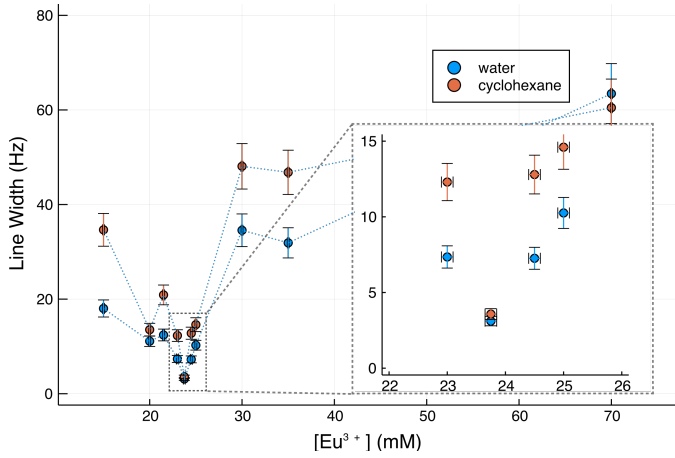


Figure 6: Observed line widths of water (blue circles) and cyclohexane (orange circles) in microfluidic droplet emulsions as a function of the Eu[DTPA]²⁻ concentration in the aqueous phase. Inset is the plot around the minimum concentration. The widths of both lines are minimal at the matched concentration of 23.75 mM.

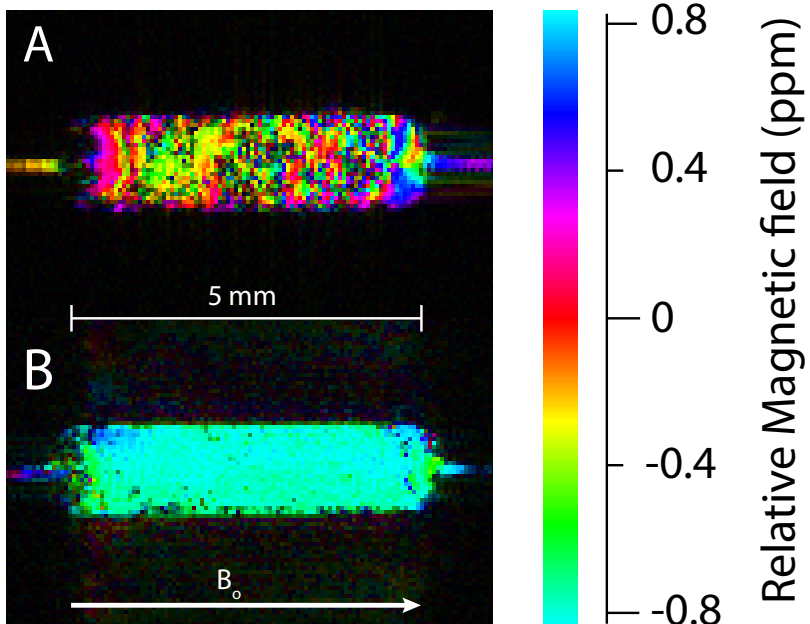


Figure 7: B_0 Field maps obtained by magnetic resonance imaging of emulsions with (A) $\Delta\chi = -1.41 \times 10^{-6}$ and (B) $\Delta\chi \approx 0$.

208 movement of the droplets is not regular. However, at high droplet densities,
 209 it can be expected to approximate a dense packing of spheres. In order
 210 to obtain a semi-quantitative prediction, we have computed the demag-
 211 netising field in face-centred cubic (FCC) and simple cubic (SC) lattices
 212 of diamagnetic spheres; the results are shown in Fig. 3. A single unit
 213 cell containing one (SC) or two (FCC) independent spheres was meshed
 214 under periodic boundary conditions in all directions (Fig. 3C). As is well
 215 known, the demagnetising field inside an isolated diamagnetic sphere is
 216 homogeneous, while the field outside of the sphere is that of a magnetic
 217 point dipole located at the sphere's centre. This situation is approxi-
 218 mated in a lattice if the lattice constant is much larger than the sphere
 219 diameter. The computed demagnetising field of a small sphere in an SC
 220 lattice is shown in Fig. 3A. The contour levels display the z -component
 221 of the local demagnetising field normalised by the background B_0 field
 222 and the susceptibility difference $\Delta\chi = \chi_{\text{sphere}} - \chi_{\text{continuous}}$. The field
 223 is homogeneous inside the sphere, and a spatially varying demagnetis-
 224 ing field only exists in the continuous phase. By contrast, in a densely
 225 packed face-centered cubic lattice the field is no longer homogeneous in-
 226 side the spheres (Fig. 3B). The FCC lattice approximates the geometry
 227 of a dense microemulsion of homogenous water-in-oil droplets. Fig. 3D
 228 shows the histograms of the z -components of the demagnetising field in
 229 the continuous and droplet phases of the FCC lattice, respectively.

230 The NMR spectra expected from an ideal emulsion of the same geom-
 231 etry can be predicted from these histograms (neglecting no broadening
 232 contributions from the sample container). The magnetic field relevant
 233 for nuclear Larmor precession, often referred to as the "external" field³⁵
 234 \mathbf{B}_{ext} is given by²⁴

$$\mathbf{B}_{\text{ext}}(\mathbf{r}) = B_0(1 + \frac{\chi_s}{3})\mathbf{e}_z - \mu_0 \nabla U_d(\mathbf{r}), \quad (1)$$

235 where B_0 is the magnitude of the external field, χ_s is the local mag-

236 netic susceptibility, and $U_d(\mathbf{r})$ is the scalar magnetic potential of the
237 demagnetising field. The volume susceptibility of a solution containing
238 a paramagnetic species at low concentration c_p is

$$\chi_s \approx \chi_0 + c_p \zeta_P, \quad (2)$$

239 where χ_0 is the volume susceptibility of the pure solvent, and ζ_P is the
240 molar susceptibility of the paramagnetic species. ζ_P depends slightly on
241 the molecular environment. For example, values of $5.86 \cdot 10^{-5}$ l/Mol,
242 $5.68 \cdot 10^{-5}$ l/Mol, and $6.14 \cdot 10^{-5}$ l/Mol have been measured at 300K
243 for Eu_2O_3 , EuF_3 , and EuBO_3 , respectively.³⁶ To our knowledge, the
244 precise molar susceptibility of $\text{Eu}[\text{DTPA}]^{2-}$ in aqueous solution has not
245 been measured to date, but it is likely to be similar to the above values.

246 Fig. 4 shows ^1H NMR spectra obtained from emulsions in the chip
247 shown in Fig. 1 with varying $\text{Eu}[\text{DTPA}]^{2-}$ concentrations in the aqueous
248 phase as indicated in the figure. While the spectra are extremely broad
249 without dopant, concentrations in the vicinity of 23 mM lead to much
250 sharper lines for both water and cyclohexane, and the pure phase line
251 widths are recovered at the optimum concentration of $c_p = 23.75$ mM.

252 Using the susceptibilities given in Table 1, this leads to molar suscepti-
253 bility for $\text{Eu}[\text{DTPA}]^{2-}$ of $5.94 \cdot 10^{-5}$ l/Mol, well within the range of molar
254 susceptibilities reported in literature for other Eu^{3+} compounds. Using
255 this value, the histograms shown in Fig. 3D can be converted into pre-
256 dicted emulsion NMR spectra as a function of $\text{Eu}[\text{DTPA}]^{2-}$ concen-
257 tration in the aqueous phase, as shown in Fig. 5. The predicted behaviour
258 is qualitatively similar to the experimental observation; very broad lines
259 are expected at zero dopant concentration, while sharp lines are recov-
260 ered near the optimum concentration. Also, the droplet phase peak is
261 predicted to be narrower than the one from the continuous phase; this is
262 already evident in the histograms in Fig. 3. However, the predicted spec-
263 tra are consistently sharper than the experimentally observed ones. It is

not entirely clear what causes the discrepancy between the experimental observation and the simulations. However, it should be noted that the experimental geometry of the emulsion differs significantly from the simulation; the droplets are neither uniform in size, nor are they arranged in a crystalline (FCC) lattice.

The observed widths of the NMR signals from cyclohexane and water are summarised in Fig. 6. Here, we define the line width as the ratio of the peak integral to the peak height, multiplied by $2/\pi$. In the case of Lorentzian line shapes, this definition is equivalent to the full width at half height (FWHM). However, the expected line shapes from the droplet emulsion are very different from a Lorentzian (Fig. 3D), such that using the FWHM would be misleading.

Both line widths exhibit a narrow minimum at 23.75 mM Eu[DTPA]²⁻ in the aqueous phase. The water and cyclohexane minimum peak widths are 3.1 Hz and 3.5 Hz, respectively. For comparison, the best resolution that has been reached with the same NMR probe is 1.76 Hz for a homogeneous solution of 150 mM sodium acetate in H₂O.¹⁴

Fig. 7 shows magnetic field (B_0) maps of the sample chambers filled with droplet emulsions. In these experiments, two separate images with different echo times are acquired. The phase difference in each pixel is proportional to the echo time difference and to the local magnetic field. The echo time difference is constant therefore the colour denotes the phase acquired by each pixel and can be used to inform on the homogeneity of the magnetic field in the sample.

In Fig. 7A, the droplets do not contain any paramagnetic dopant. As a result, the susceptibilities of the phases are unmatched, and strong local magnetic field differences are visible in the images. By contrast, the droplets in Fig. 7B are doped with 23.75 mM Eu[DTPA]²⁻. As is clearly visible in the image, the local differences in the magnetic fields are strongly attenuated in this case.

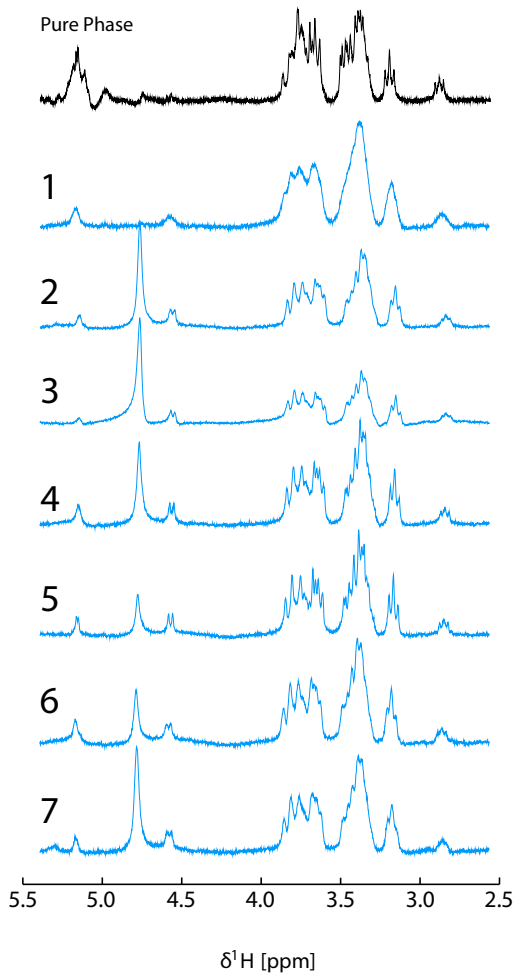


Figure 8: Spectra of 200 mM Glucose in H_2O obtained from microfluidic droplet emulsions in cyclohexane. 1: Aqueous phase contains $c_0 = 23.75 \pm 0.25$ mM $\text{Eu}[\text{DTPA}]^{2-}$. Spectra 2-7 have been obtained by gradual dilution of the aqueous phase with small amounts of DI water. 2: $\ln c/c_0 = -0.5\%$; 3: $\ln c/c_0 = -0.75\%$; 4 : $\ln c/c_0 = -0.875\%$; 5 : $\ln c/c_0 = -1.0\%$; 6 : $\ln c/c_0 = -1.125\%$; 7 : $\ln c/c_0 = -1.25\%$. A spectrum of pure phase 200mM glucose with optimised Eu doping in the same chip is included for comparison (black). The nonuniform peak at 4.8 ppm is due to carrier frequency drift during water suppression

294 While the above results have demonstrated that optimal line widths
295 can be minimised in ^1H NMR spectra of microfluidic emulsions by para-
296 magnetic doping, the question remains if this is sufficient to resolve
297 homonuclear J -couplings of a few Hz. This is required in order to do
298 meaningful NMR spectroscopy, particularly in the context of complex
299 metabolic mixtures. The top trace in Fig. 8 shows a spectrum of 200
300 mM glucose and 23.75 mM Eu[DTPA] $^{2-}$ in water. The water signal has
301 been suppressed by pre-saturation. In this case, the resolution is about
302 3 Hz; such that e.g., the triplet at 3.2 ppm (which corresponds to the
303 proton in the 2-position on the β -glucose anomer) is clearly resolved.

304 Spectrum 1 in Fig. 8 has been obtained from droplet emulsions, start-
305 ing form an aqueous stock solution prepared to a nominal concentration
306 of 23.75 mM in Eu[DTPA] $^{2-}$ and 200 mM in glucose. To our initial dis-
307 appointment, the resolution in this spectrum is quite poor, in spite of the
308 attempt to dope at the previously determined optimum concentration.
309 However, we estimate the pipetting and weighing errors to add up to an
310 uncertainty in the concentration of the stock solution of $\pm 1\%$. Assuming
311 the stock solution was too concentrated, rather than too dilute, it was
312 then gradually diluted with small amounts of DI water corresponding
313 to a change in concentration much less than the experimental error in
314 each step. As can be seen in spectra 2-7, the resolution gradually in-
315 creases, and matches the pure phase spectrum at spectrum 5, before it
316 deteriorates again. In practice, high resolution spectra therefore require
317 careful calibration of the dopant concentration. It may not be practical
318 to achieve this in one step by preparing the stock solution, particularly
319 if small volumes (around 10 ml or so) are used as in our experiments.
320 Rather, a gradual dilution as in Fig. 8 may be required to calibrate the
321 Eu[DTPA] $^{2-}$ concentration for an accurate match of the aqueous and
322 carrier fluid susceptibilities. However, if such a match is established, the
323 resulting resolution is as good as that of the pure aqueous solution.

324 In summary, we have shown that the susceptibility differences be-
325 tween the chip, the aqueous phase, and the oil phase in a microfluidic
326 droplet system can be successfully mitigated by a combination of struc-
327 tural shimming and doping of the less diamagnetic of the liquid phases
328 with a europium compound. The ultimate resolution achieved is only
329 slightly inferior to what has been demonstrated in homogeneous solu-
330 tions on a microfluidic chip and is suitable for high resolution NMR
331 spectroscopy.

332 This work has been supported by the 7th EU Framework programme
333 through a Marie Curie Career Integration Fellowship to MU, and by
334 the Horizon 2020 FETOPEN project TISuMR. The authors are grateful
335 to Visvaldis Buns and Ali Yilmaz for help with manufacturing of the
336 microfluidic chip.

337 References

- 338 [1] N. Aranibar, M. Borys, N. A. Mackin, V. Ly, N. Abu-Absi, S. Abu-Absi, M. Niemitz,
339 B. Schilling, Z. J. Li, B. Brock, R. J. I. Russell, A. Tymiak and M. D. Reily, *Journal*
340 *of Biomolecular NMR*, 2011, **49**, 195–206.
- 341 [2] D. S. Wishart, *TrAC Trends in Analytical Chemistry*, 2008, **27**, 228–237.
- 342 [3] T. Thorsen, R. W. Roberts, F. H. Arnold and S. R. Quake, *Phys Rev Lett*, 2001, **86**,
343 4163–4166.
- 344 [4] S. L. Anna, N. Bontoux and H. A. Stone, *Applied Physics Letters*, 2003, **82**, 364–366.
- 345 [5] A. Günther and K. Jensen, *Lab Chip*, 2006, **6**, 1487–1503.
- 346 [6] P. Garstecki, M. J. Fuerstman, H. A. Stone and G. Whitesides, *Lab Chip*, 2006, **6**,
347 693–693.
- 348 [7] T. P. Lagus and J. F. Edd, *J. Phys. D Appl. Phys.*, 2013, **46**, 114005.
- 349 [8] L. Mazutis, J. Gilbert, W. L. Ung, D. A. Weitz, A. D. Griffiths and J. A. Heyman,
350 *Nat Protoc*, 2013, **8**, 870–891.
- 351 [9] A. B. Theberge, E. Mayot, A. El Harrak, F. Kleinschmidt, W. T. S. Huck and A. D.
352 Griffiths, *Lab Chip*, 2012, **12**, 1320–1326.
- 353 [10] Y. Zhu and Q. Fang, *Analytica Chimica Acta*, 2013, **787**, 24–35.
- 354 [11] V. Badilita, R. C. Meier, N. Spengler, U. Wallrabe, M. Utz and J. G. Korvink, *Soft*
355 *Matter*, 2012, **8**, 10583–10597.

- 356 [12] S. S. Zalesskiy, E. Danieli, B. Blümich and V. P. Ananikov, *Chem. Rev.*, 2014, **114**,
357 5641–5694.
- 358 [13] N. Spengler, J. Höfflin, A. Moazenzadeh, D. Mager, N. MacKinnon, V. Badilita,
359 U. Wallrabe and J. G. Korvink, *Plos One*, 2016, **11**, e0146384.
- 360 [14] G. Finch, A. Yilmaz and M. Utz, *Journal of Magnetic Resonance*, 2016, **262**, 73–80.
- 361 [15] P. W. Kuchel, B. E. Chapman, W. A. Bubb, P. E. Hansen, C. J. Durrant and M. P.
362 Hertzberg, *Concepts in Magnetic Resonance Part A*, 2003, **18A**, 56–71.
- 363 [16] C. J. Durrant, M. P. Hertzberg and P. W. Kuchel, *Concepts Magn. Reson.*, 2003,
364 **18A**, 72–95.
- 365 [17] J. C. VANDENENDEN, D. WADDINGTON, H. VANAALST, C. G. VANKRALIN-
366 GEN and K. J. PACKER, *Journal of Colloid and Interface Science*, 1990, **140**,
367 105–113.
- 368 [18] I. FOUREL, J. P. GUILLEMENT and D. LEBOTLAN, *Journal of Colloid and In-*
369 *terface Science*, 1994, **164**, 48–53.
- 370 [19] K. G. Hollingsworth, A. J. Sederman, C. Buckley, L. F. Gladden and M. L. Johns,
371 *Journal of Colloid and Interface Science*, 2004, **274**, 244–250.
- 372 [20] J. P. Hindmarsh, J. H. Su, J. Flanagan and H. Singh, *Langmuir*, 2005, **21**, 9076–9084.
- 373 [21] M. L. Johns, *Current Opinion in Colloid & Interface Science*, 2009, **14**, 178–183.
- 374 [22] R. Bernewitz, G. Guthausen and H. P. Schuchmann, *Magnetic Resonance in Chem-*
375 *istry*, 2011, **49**, S93–S104.
- 376 [23] I. A. Lingwood, T. C. Chandrasekera, J. Kolz, E. O. Fridjonsson and M. L. Johns,
377 *Journal of Magnetic Resonance*, 2012, **214**, 281–288.
- 378 [24] H. Ryan, A. Smith and M. Utz, *Lab Chip*, 2014, **14**, 1678–1685.
- 379 [25] M. E. Fabry and R. C. San George, *Biochemistry*, 1983, **22**, 4119–4125.
- 380 [26] A. J. Lennon, N. R. Scott, B. E. Chapman and P. W. Kuchel, *Biophysical journal*,
381 1994, **67**, 2096–2109.
- 382 [27] J. A. Peters, J. Huskens and D. J. Raber, *Progress in Nuclear Magnetic Resonance*
383 *Spectroscopy*, 1996, **28**, 283–350.
- 384 [28] *CRC Handbook of Chemistry and Physics*, ed. J. Rumble, 2017, pp. 1–4.
- 385 [29] M. C. Wapler, J. Leupold, I. Dragonu, D. von Elverfeld, M. Zaitsev and U. Wallrabe,
386 *Journal of Magnetic Resonance*, 2014, **242**, 233–242.
- 387 [30] C. J. G. Bakker and R. de Roos, *Magn. Reson. Med.*, 2006, **56**, 1107–1113.
- 388 [31] A. Yilmaz and M. Utz, *Lab Chip*, 2016, **16**, 2079–2085.
- 389 [32] G. R. Finch, *PhD thesis*, University of Southampton, Southampton, 2017.

- 390 [33] J. Bezanson, A. Edelman, S. Karpinski and V. B. Shah, *SIAM Rev.*, 2017, **59**, 65–98.
- 391 [34] COMSOL Inc., *COMSOL Multiphysics®*, <https://www.comsol.com>.
- 392 [35] M. H. Levitt, *Concepts Magn. Reson.*, 1996, **8**, 77–103.
- 393 [36] Y. Takikawa, S. Ebisu and S. Nagata, *Journal of Physics and Chemistry of Solids*,
- 394 2010, **71**, 1592–1598.